forests

MDPI

*Article*

# Effect of Applied Pressure on the Performance of Biodegradable Fiber Insulation Board Manufactured from Camphor Branches (*Cinnamomum camphora*)

**Ziyi Cai [1,†], Xiaowen Song [2,†], Xiulun Wang [1,*], Tongxin Guo [3], Hiroshi Takahashi [4] and Changqing Cai [5,*]**

[1] Graduate School of Bioresources, Mie University, 1577 Kurimamachiya-cho, Tsu 5148507, Japan; 522d202@m.mie-u.ac.jp
[2] College of Mechanical Engineering, Inner Mongolia University of Technology, Hohhot 010051, China; sxw_istgut@imut.edu.cn
[3] Graduate School of Regional Innovation Studies, Mie University, 1577 Kurimamachiya-cho, Tsu 5148507, Japan; 622d0s1@m.mie-u.ac.jp
[4] Graduate School of Maritime Sciences, Kobe University, 5-1-1 Fukaeminami-machi, Kobe 6580022, Japan; 203w951w@stu.kobe-u.ac.jp
[5] College of Electrical and Information Engineering, Changchun Institute of Technology, 395 Kuanping Road, Changchun 130103, China
* Correspondence: wang@bio.mie-u.ac.jp (X.W.); caicq@ccit.edu.cn (C.C.)
† These authors contributed equally to this work.

**Abstract:** Currently, the predominant thermal insulation materials in the construction industry are primarily derived from inorganic sources. While these materials demonstrate commendable thermal insulation capabilities, their widespread use raises significant environmental concerns. The utilization of wood fiber materials presents a promising solution to mitigate these drawbacks. This study focuses on the fabrication of biodegradable fiber insulation board (BFIB) using camphor branches. The manufacturing process avoids the use of chemical additives, employing a physical method that utilizes hot pressing and relies on the formation of intermolecular hydrogen and hydroxide bonds between the fibers. The study evaluates the influence of applied pressure on the properties of BFIB. SEM images reveal that, with an increase in applied pressure, the fibers exhibit a more regular pattern, subsequently enhancing the mechanical properties, hygric behavior, and fire resistance properties of BFIB. As an environmentally friendly and renewable material, BFIB holds the potential to substitute conventional insulation materials. It is particularly intriguing for energy-saving purposes when applied as building insulation for walls or ceilings.

**Keywords:** binderless fiberboard; renewable resources; hygrothermal; wood waste; thermal insulation

check for updates

**Citation:** Cai, Z.; Song, X.; Wang, X.; Guo, T.; Takahashi, H.; Cai, C. Effect of Applied Pressure on the Performance of Biodegradable Fiber Insulation Board Manufactured from Camphor Branches (*Cinnamomum camphora*). *Forests* **2024**, *15*, 156. https://doi.org/10.3390/f15010156

Academic Editor: Luis García Esteban

Received: 4 December 2023
Revised: 19 December 2023
Accepted: 26 December 2023
Published: 11 January 2024

**Copyright:** © 2024 by the authors. Licensee MDPI, Basel, Switzerland. This article is an open access article distributed under the terms and conditions of the Creative Commons Attribution (CC BY) license (https://creativecommons.org/licenses/by/4.0/).

## 1. Introduction

Japan, which is located in the Pacific Rim seismic zone and characterized by a temperate oceanic monsoon climate, extensively incorporates wood materials in its construction practices due to geographical considerations. However, contemporary architectural designs in Japan have gradually shifted away from the traditional, climate-responsive principles, embracing Western architectural influences. This evolution inevitably compromises the inherent ability of dwellings to naturally regulate the internal environmental conditions, necessitating the widespread installation of mechanical air conditioning systems [1]. Notably, as was reported by the Japan Agency for Natural Resources and Energy (METI) in 2018, air conditioning systems contributed to approximately 20.3% of the total annual energy consumption [2].

Addressing the energy demand of air conditioning involves the incorporation of thermal insulation into the building envelope [1]. Thermal insulation materials, as the largest building components, play a crucial role in enhancing the energy efficiency of buildings. A

myriad of thermal insulation types are currently available for use in construction, which can be categorized as follows: (1) inorganic materials encompassing fibrous selections like glass, rock, and slag wool, alongside cellular options like calcium silicate, bonded perlite, vermiculite, and ceramic products; (2) organic materials encompassing fibrous options such as cellulose, cotton, wood, pulp, cane, and synthetic fibers, as well as cellular choices like cork, foamed rubber, polystyrene, polyethylene, polyurethane, polyisocyanurate, and other polymers; and (3) metallic or metalized reflective membranes, which must incorporate air-filled, gas-filled, or evacuated space to be effective [3]. Fibers are widely acknowledged for their application as insulating materials derived from renewable resources. They possess intrinsic features such as a hollow structure, low density, and remarkable thermal insulation properties, aligning with the principles of sustainable human development [4].

It has been reported in the literature that the typical thermal conductivity values for cellulose insulation materials fall within the range of 0.04 to 0.05 W/(m·K) [5]. Khedari et al. [6,7] pioneered the development of an economically efficient particleboard composed of a blend of durian peel and coconut coir. This innovation resulted in a material configuration with reduced thermal conductivity, rendering it particularly effective for applications such as insulation for ceilings and walls, in terms of energy conservation. Binici et al. [8] employed sunflower stalks and cotton textile waste to develop thermal insulation materials, utilizing epoxy as a binding agent. The experimental findings indicate that the specimens containing sunflower stalks with cottony fibers exhibit notably reduced heat transfer coefficients. This approach offered valuable insights for the fabrication of construction materials while concurrently mitigating the environmentally problematic waste materials. In another interesting work, Paiva et al. [9] established an unconventional yet accelerated experiment aimed at assessing the thermal insulation capabilities of corn cob particleboards bonded together with wood glue. This evaluation was conducted within the context of authentic thermal and hygrometric conditions. Currently, there is an increasing array of globally successful projects, which serves as a testament to the viability of utilizing plant fibers in building envelope insulation [10,11]. The merits of fiber-based materials, compared to conventional insulation materials, encompass their biodegradable nature, cost-effectiveness, and ready availability.

Nevertheless, the insulation boards investigated in the aforementioned works incorporate diverse chemical additives to varying extents, rendering them unsuitable for direct burial or disposal upon use. Meanwhile, the predominant emphasis in these investigations has revolved around the assessment of the thermal and mechanical characteristics of these materials, while their hygric behaviour and fire resistance have been scarcely examined. It is also worth noting that most of non-wood biomass materials (straw, stalk, bagasse, and stem) have a small diameter and are more suitable as a raw material for particleboard production. Wood biomass can be easily obtained as a homogeneous material, in terms of pellet size and shape, and the randomness of the arrangement leads to the development of homogeneous voids between them more easily [12,13].

Along these lines, the goal of this work was to delve into the utilization of forestry, pruning branches as a primary resource for insulating building envelopes, specifically assessing their hygric behaviour and fire resistance. In addition, their thermal and mechanical properties were comprehensively characterized. Presently, wood fiber is predominantly employed in the production of fiber insulation boards through the addition of a limited quantity of PUR resin via a dry process, resulting in thermal conductivity values ranging from 0.037 to 0.05 W/(m·K) [14]. This method continues to encounter environmental challenges, particularly regarding the management of subsequent disposal.

To effectively address this issue, our work pioneered a sustainable approach by manufacturing BFIB using the wet method, omitting the incorporation of chemical additives during the production process. BFIB solely relies on hydrogen bonding between fiber molecules for cohesion, offering a potential solution for direct disposal after use by using burial or alternative methods. A deep understanding of the significant factors affecting the performance of fiber insulation boards, such as applied pressure, heating temperature,

and heating time, is also of crucial importance. The thermal insulation attributes of BFIB are partly contingent upon porosity, with the magnitude of the applied pressure playing a direct role in affecting the material's porosity. To this end, in this work, the applied pressure magnitude during the manufacturing process of BFIB was systematically altered, aiming to explore its potential utility within the realm of thermal insulation materials. The viability of pruned branches as a primary resource for building envelope insulation was also explored, addressing environmental challenges and providing insights into sustainable construction practices. Our work provides valuable insights for the development of next-generation eco-friendly building materials, tackling the pressing challenges associated with energy consumption, waste management, and environmental impact in the construction industry.

## 2. Materials and Methods

### 2.1. Materials

The biodegradable fiber insulation board (BFIB) was manufactured using camphor tree pruned branches sourced from the Mie University campus and water from the municipal network. Initially, during the fabrication of the branches, they were air-dried until reaching a moisture content below 6.5%, as shown in Figure 1a. Subsequently, the leaves were separated and buried in the soil, resulting in the camphor pruned branches illustrated in Figure 1b. These branches were then further processed into small chips, approximately 1 cm in size, using an electric disintegrator (Cowa Cutter Co., Shizuoka, Japan) operating at 900 rpm.

(**a**) (**b**)

**Figure 1.** Camphor tree pruned branches used for manufacturing the BFIB. (**a**) Pruned branches on campus; (**b**) pruned branches with leaves removed.

### 2.2. Composition Analysis

In this work, the Van Soest analysis method was employed to determine the composition of camphor pruning residues [15]. The Van Soest analysis process involved the progressive separation of camphor branches into neutral detergent solution fiber (NDSF), acid detergent solution fiber (ADSF), and strong acid fiber (SASF). Generally, NDSF comprises hemicellulose, cellulose, lignin, and insoluble minerals, while ADSF is primarily composed of cellulose, lignin, and insoluble minerals. In contrast, SASF exclusively comprises lignin and insoluble minerals. The lignin content in the SASF fraction was determined by subtracting the ash weight. All results were expressed as a percentage of the overall dry weight. The amounts of cellulose and hemicellulose (in %) can be calculated using the following relations [16]:

$$\text{Hemicellulose (\%)} = \text{NDSF (\%)} - \text{ADSF (\%)} \quad (1)$$

$$\text{Cellulose (\%)} = \text{ADSF (\%)} - \text{Lignin (\%)} \quad (2)$$

### 2.3. The Process of Manufacturing BFIB

An innovative manufacturing process for BFIB employing exclusively physical methods was introduced here. More specifically, the procedure involved immersing tiny chips

in water at 25 °C for one month under standard room temperature and pressure conditions. This leads to a thorough water absorption and expansion of the tiny chips. Subsequently, the saturated tiny chips were processed in a refining machine (Satomi Corp., Shizuoka, Japan), utilizing water as the circulating medium at a 5% concentration. The water pressure was maintained at 0.4 MPa, with a flow rate of 10 L/min during operation. During this process, the tiny chips from camphor branches were physically dissociated into individual fibers, each measuring 3 mm in length. These fibers were next configured into an aqueous fiber pulp at a concentration of 0.05 g/mL through the addition of water. The pH of the aqueous fiber pulp was measured to be 7.53 using a pH meter (DKK-TOA Co., Tokyo, Japan). During the subsequent dry molding process, 500 mL of the fiber pulp was deposited into a metal mold measuring 100 mm in length and width. To simultaneously apply pressure and heat to the fiber pulp, a manually controlled hydraulic press system was employed in conjunction with a hot press (Imoto Machinery Co., Kyoto, Japan). The experimental conditions for manufacturing BFIB are outlined in Table 1. The target density of the BFIB was above 0.8 g/cm$^3$. Through several experiments, it was found that when the applied pressure was less than 2 MPa, the target density of BFIB was difficult to meet. Therefore, the minimum applied pressure in this work was 2 MPa, and then was sequentially increased. A continuous increase in the pressure did not improve the performance consistently. For this reason, the maximum applied pressure was kept at 8 MPa.

**Table 1.** Experimental conditions for the fabrication of BFIB.

| Applied Pressure | Heating Temperature | Hot-Press Time |
|---|---|---|
| 2.0 MPa<br>3.5 MPa<br>5.0 MPa<br>6.5 MPa<br>8.0 MPa | 110 °C | 2.0 h |

The applied pressure plays a dual role: first, water molecules bound to the fiber molecules are detached, and, simultaneously, the proximity of dehydrated fiber molecules is promoted, facilitating the creation of fresh chemical bonds through hydrogen and hydroxide bonding. Subsequently, the application of heat results in the expulsion of the detached water molecules in the form of water vapour, leading to the formation of BFIB approximately 2 mm in thickness. Finally, the manufactured BFIB undergoes drying within a controlled temperature dryer (IUCHI Corp., Tokushima, Japan) at 105 °C for half an hour. This step aims to eliminate any remaining moisture within the BFIB's internal voids, enhancing porosity, and, consequently, lowering the thermal conductivity.

### 2.4. Microstructure Study

For a comprehensive examination of the surface and internal fiber arrangement structure of BFIB, samples measuring 1.0 cm × 1.0 cm were precisely cut using an ultrasonic cutter (Honda Plus, Shinshiro, Japan). This equipment ensured the creation of smooth surface cross-sections, enabling detailed microstructure observations of BFIB. Given the inherent lack of electrical conductivity in plant fibers, a gold spray coating was applied to the BFIB samples before the observation. Subsequently, the Sigma 300 instrument (Carl Zeiss AG, Jena, Germany) was employed to magnify the gold-sprayed BFIB samples at a 500× magnification, all conducted under vacuum conditions. Notably, this instrument was equipped with a Gemini lens, facilitating the detection of both secondary electrons (SE) and backscattered electrons (BSE).

### 2.5. Characterization of the Crystallinity

Wide-angle X-ray diffraction (XRD) was employed to investigate the influence of the varying applied pressures on the crystallinity index of cellulose in BFIB. Prior to analysis, BFIB was meticulously sectioned into 1.5 cm × 1.5 cm specimens. X-ray diffraction (XRD)

experiments were conducted using a high-resolution (HR) diffractometer (Rigaku Co., Tokyo, Japan) with a Cu-Kα1 radiation source (λ = 0.15406 nm) at an operating voltage and current of 40 kV and 30 mA, respectively. To enhance accuracy, a fine nickel filter efficiently eliminated Cu K1 radiation. The XRD scans were performed in the reflection mode, covering a 2θ angle range from 3° to 80° and scanned at a rate of 5°/min. To assess the crystallinity index of the specimens, the widely recognized Segal method was applied, a standard technique for measuring crystallinity in cellulose samples [17,18]. The crystallinity index (CrI) can be defined as follows:

$$CrI = 100\% \times (I_{002} - I_{am})/I_{002} \quad (3)$$

where CrI represents the relative degree of crystallinity, $I_{002}$ denotes the maximum intensity of the principal peak (002) lattice diffraction, and $I_{am}$ refers to the diffraction intensity of amorphous cellulose between the plane (200) and (110). $I_{002}$ represents both the crystalline and amorphous regions, while $I_{am}$ describes only the amorphous region.

### *2.6. Compaction Rate*

The compaction rate of BFIB in this work was determined by evaluating its porosity. More specifically, the porosity of BFIB was calculated by measuring both its apparent and true densities. To determine the apparent density of BFIB, a density profile analyser (Electronic Wood Systems, Hameln, Germany) with a sample size of 50 mm × 50 mm was employed. This instrument facilitated the measurement of the density distribution across the entire thickness of the sample. The measurement process to determine the apparent density of BFIB was both non-destructive and non-contact, relying on X-ray technology. Meanwhile, the true density of BFIB was determined through a density analyser (Kunshan Lugong Precision Instrument Co., Kunshan, China). This instrument relied on buoyancy measurements, employing Archimedes' principle to calculate BFIB's true volume. The sample size for this measurement was 25 mm × 25 mm. The porosity was computed using Equation (4).

$$P = (1 - \rho_1/\rho_2) \times 100\% \quad (4)$$

where P is the porosity of the samples, $\rho_1$ stands for the apparent density of the samples, and $\rho_2$ denotes the true density of the samples.

### *2.7. Bonding Strength Test*

BFIB underwent a series of tests, including three-point bending, tensile, internal bond strength (IBS), and screw-holding force (SHF) tests, utilizing a universal testing machine (IMADA Co., Toyohashi, Japan) in accordance with the JIS-A5905: Fiberboards 2014 [19] standard. BFIB specimens were prepared as depicted in Figure 2a,b, and the BFIB's modulus of elasticity was determined by conducting bending and tensile tests, applying the calculation formulas presented in Equations (5) and (6).

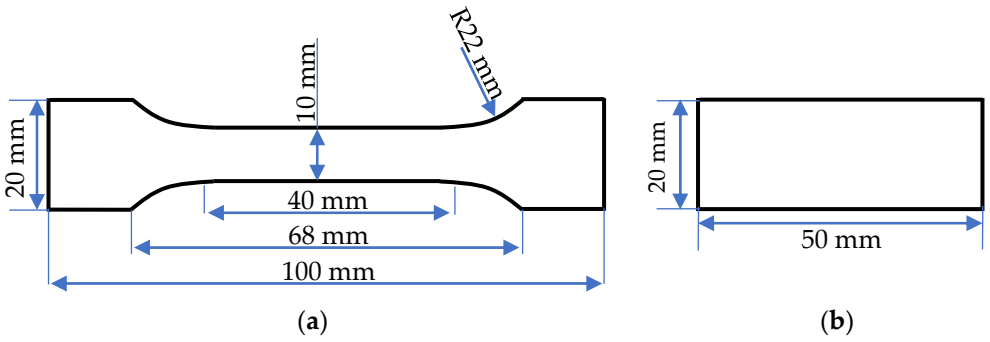


**Figure 2.** The specimens for the test: (**a**) tensile test; (**b**) bending test.

BFIB was cut into 50 mm × 50 mm specimens, and six of these specimens were stacked to ensure a thickness exceeding 11 mm. Wood screws were then employed to affix the stacked specimens, and the maximum force required to extract the screws was measured as the screw-holding force. During the bending test, the crosshead was lowered at a consistent rate of 15 mm/min. For both the tensile test and screw-holding force tests, the experimental speed was set at 15 mm/min in the upward direction. In the internal bond strength test, specimens measuring 50 mm × 50 mm were excised from BFIB. A uniform application of epoxy-resin-based adhesive (KONISHI Co., Osaka, Japan) was made to both sides of the BFIB specimens. Subsequently, these specimens were securely clamped between two metal hooks on a universal testing machine, and a load was applied at a rate of 2 mm/min. The internal bond strength was calculated using Equation (7). For each test, 15 distinct sets of BFIB that were produced under varying conditions were prepared for examination.

$$MOE_B = (L^3 \cdot F)/(4a \cdot b^3 \cdot \Delta L) \quad (5)$$

$$MOE_T = F \cdot L/(a \cdot b \cdot \Delta L) \quad (6)$$

$$IB = F/h^2 \quad (7)$$

where $MOE_B$ is the bending modulus of elasticity, $MOE_T$ denotes the tensile modulus of elasticity L is the supported span, $F$ states the applied load, a represents the width of the specimen, b is the thickness of the specimen, ΔL signifies the amount of change in the displacement, $S$ is the cross-sectional area of the specimen, and $H$ stands for the gauge length of the specimen.

### 2.8. Moisture Resistance

It is well-known that the moisture vapour barrier properties play a crucial role in building material applications [20]. To assess the water vapour transmission properties of the materials, the cup method outlined in JIS Z 0208 [21] was employed. This method requires a minimum moisture-permeable area of 25 cm × 25 cm and a maximum thickness of 3 mm for the test specimen. Circular samples, measuring 60 mm in diameter and 3 mm in thickness, were hermetically sealed with silicone at the upper limit of a glass jar's opening. A screw lid with a 62 mm aperture was affixed to the assembly. Beneath the test specimen, desiccant was uniformly positioned 3 mm from the lower surface. The dish assembly was weighed before being introduced into a controlled chamber set at 75% relative humidity (RH) and 20 °C. Periodic measurements of weight and time were recorded. A total of ten experimental sets were conducted for each set of conditions. The water vapour transmission rate (WVTR) was computed using Equation (8), while the water vapour permeance (WVP) was calculated employing Equation (9):

$$WVTR = (G/t)/A \quad (8)$$

$$WVP = WVTR/\Delta p = WVTR/S\,(R_1 - R_2) \quad (9)$$

where WVTR represents the water vapour transmission rate, G denotes the weight change, t is the test time, G/t refers to the slope of the straight line, and A is the test area. Moreover, WVP represents the water vapour permeance, Δp is the vapour pressure difference, S states the saturation vapor, $R_1$ is the relative humidity at the source expressed as a fraction (the test chamber for desiccant method; in the dish for water method), and $R_2$ signifies the relative humidity at the vapour sink expressed as a fraction.

### 2.9. The Thermal Insulation Properties

The thermal conductivity of BFIB in this work was measured using the temperature wave analysis (TWA) method, an internationally recognized ISO 22007-6 standardized method [22] for determining thermal conductivity. The thermal conductivity analyser (ai-Phase Co., Tokyo, Japan) employed in our research can generate temperature waves

with amplitudes ranging from 0.001 to 1 Hz at 20 °C and is capable of accommodating specimen sizes of 3.0 mm × 6.0 mm or larger, with a minimum thickness of 1.0 mm. We conducted 10 measurements for each sample and calculated the average.

### 2.10. Fire Behavior

The limited oxygen index (LOI) test was performed in compliance with the JIS K 7201-2 standard [23] using the fire testing technology LOI instrument (Nanjing Jionglei Instrument Equipment Co., Jiangsu, China). The specimen size for LOI measurement was 80 mm × 10 mm with a maximum thickness of 10.5 mm. The analysis comprised two key stages. During the initial stage, the preliminary oxygen concentration was determined, while in the second stage, the limited oxygen index value was ascertained. The LOI value represents the minimum oxygen concentration needed in an oxygen–nitrogen mixture for at least three minutes or until the specimen has burned more than 50 mm from the top, thus, sustaining combustion. Higher LOI values signify greater flame resistance in the samples. Each type of bio-insulation board underwent testing with 15 samples.

### 2.11. Data Analysis

All the results from the production of BFIB in this work underwent rigorous statistical analysis. To evaluate the impact of the different applied pressures on the experimental outcomes of BFIB, analysis of variance (ANOVA) was employed here, which is a statistical method for comparing means among experimental groups. ANOVA tests the null hypothesis that all group means are equal. If significant variations exist across the groups, it is reasonable to infer that the experimental modifications affect the dependent variables [24].

## 3. Results and Discussion

### 3.1. Lignocellulosic Analysis

The BFIB in this work did not incorporate chemical binders, making the chemical composition of their raw materials the primary factor affecting various properties of the BFIB. The selected raw material consisted of pruned branches from camphor, distinct in chemical composition from camphor tree trunks. To understand this distinction, an analysis of the chemical composition of camphor pruned branches and trunks was performed using the Van Soest method. The results are presented in Table 2. Compared to the trunk, pruned branches contain relatively higher levels of hemicellulose and lignin, along with lower levels of cellulose, a conclusion consistent with Miranda et al. [16].

**Table 2.** Properties of materials (dry solid basis).

| | Cellulose (%) | Hemicellulose (%) | Lignin (%) | Reference |
|---|---|---|---|---|
| Camphor branches | 44.14 ± 1.01 | 20.15 ± 0.43 | 19.18 ± 1.12 | |
| Camphor trunk | 49.87 ± 1.17 | 19.98 ± 0.54 | 18.76 ± 1.03 | |
| Cotton stalk | 39.16 | 13.38 | 25.74 | [3] |
| Soybean straw | 35 | 17 | 21 | [25] |

As a woody material, camphor branches have a relatively high cellulose content, but a relatively low lignin content compared to other non-woody materials (cotton stalk, soybean straw). In the experimental conditions of the BFIB fabrication in this work, the heating temperature was relatively low and it was difficult to reach the melting point of lignin. We have to underline that the performance of the BFIB hinges primarily on the formation of hydrogen and hydroxide bonds between cellulose molecules, making the cellulose content a pivotal factor affecting their properties. Although the higher cellulose content facilitates the enhancement of the BFIB's properties, the conditions under which the BFIB are made are also one of the main factors affecting their performance.

### *3.2. SEM Imaging*

To gain a comprehensive understanding of the microstructural variations in BFIB under varying applied pressures, the surfaces and cross-sections of the boards were scrutinized using scanning electron microscopy (SEM) to analyze their morphology. Representative samples of BFIB produced under different applied pressures (2.0 MPa, 5.0 MPa, and 8.0 MPa) are highlighted in Figure 3. Upon analysing the surface microstructure of BFIB, it was observed that increasing the applied pressure led to a more orderly fiber arrangement. Beyond that, microscopic analysis of the cross-section of BFIB produced at an applied pressure of 2.0 MPa revealed an interior filled with numerous tiny voids and continuous gullies. However, as the applied pressure increased to 8.0 MPa, the tiny voids in the cross-section significantly decreased, and the depth of the gullies became shallower. This result indicates that higher applied pressure enhances mutual bonding between fibers, influencing the tiny voids within BFIB.

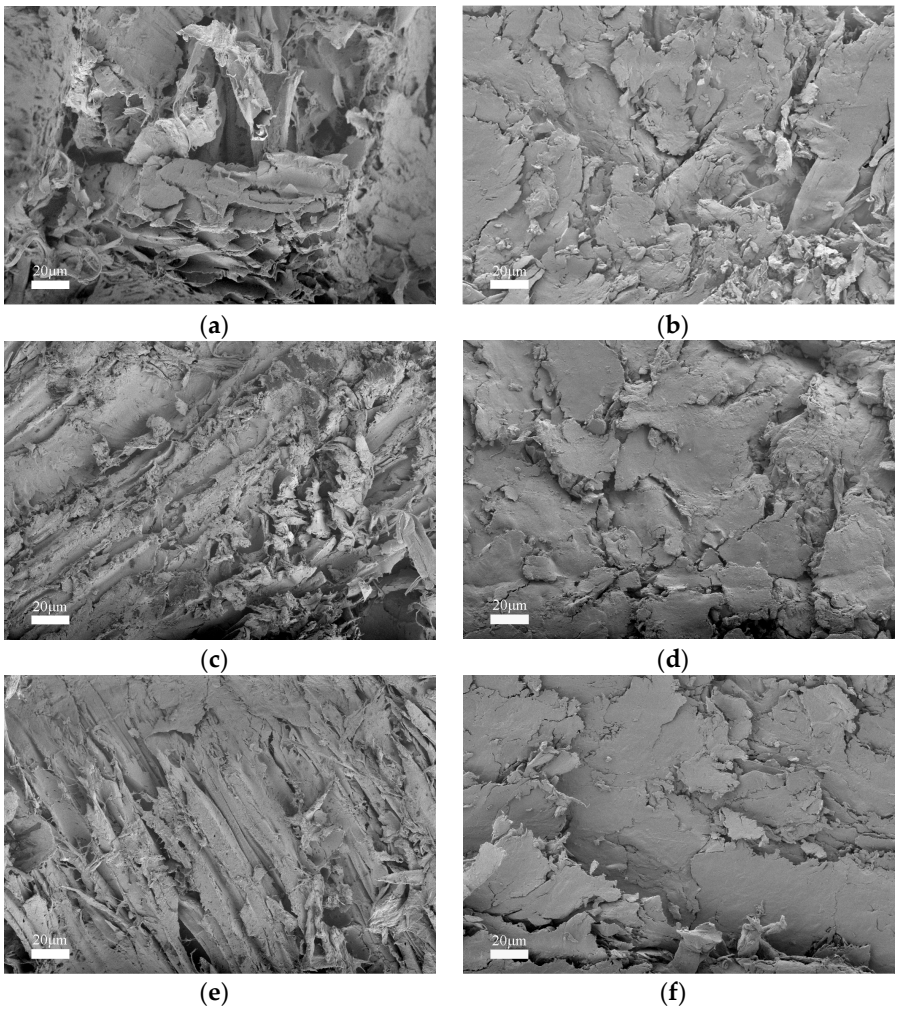


**Figure 3.** Microscopic view of the bio-insulation board (500× magnification). Surfaces: (**a**) 2.0 MPa; (**c**) 5.0 MPa; (**e**) 8.0 MPa. Section: (**b**) 2.0 MPa; (**d**) 5.0 MPa; (**f**) 8.0 MPa.

BFIB is produced by a wet process and relies primarily on a self-bonding formation mechanism. As the applied pressure increases, cellulose molecules are haphazardly stacked to form tiny voids, and hydrogen bonds are formed between free hydroxyl molecules on the fiber molecules, Nonetheless, the formation of hydrogen bonding is blocked to some extent by tiny voids. The increase in the applied pressure leads to a gradual reduction in the tiny voids on the surface and section of the BFIB. Lignin plasticizing cannot occur due to the low heating temperature. Thus, hydrogen bonding is the only bonding force, formed during

the heating and drying processes of wet process [26]. The fiber arrangement characteristics similar to those of the present study can be observed under microscopic conditions for the bamboo binderless fiberboards explored by Shi et al. [27]. Additionally, a comparative examination of the surface and section of BFIB produced under the same conditions unveiled that the fibers on the surface layer were relatively loosely arranged, exhibiting a larger number of tiny voids, potentially a result of moisture exclusion. In contrast, the internal layers of BFIB exhibited a tighter fiber bond compared to the surface layer.

### *3.3. Wide-Angle X-ray Diffraction (WAXD) Analysis*

Figure 4 illustrates the X-ray diffractograms obtained from the BFIB, revealing a consistent cellulose crystal structure in all samples, aligning with the typical cellulose type I structure. Distinct diffraction peaks near 2θ = 16.4° and 22.5° confirm the preservation of this structure [28]. Consequently, it is established that the heat-pressing process alone does not induce alterations in the crystal structure.

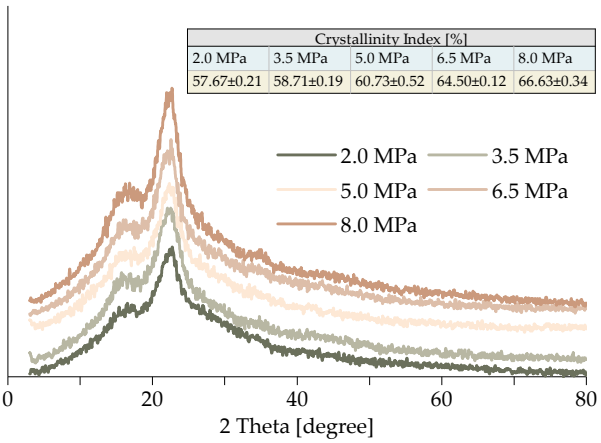


**Figure 4.** X-ray diffraction patterns obtained for the BFIB.

Crystallinity, a pivotal factor influencing wood material properties, exhibited a slight increase in cellulose within this study as applied pressure rises. The hot-pressing procedure enhanced contact forces between cellulose molecules, fostering their orderly arrangement and influencing the crystalline morphology. Thus, the intensified contact between fiber molecules amplified the potential for hydrogen bonding, prompting the transformation of the cellulose crystal structure from an α-type to a more stable β-type, consequently enhancing relative crystallinity [29]. Moreover, the degradation of hemicellulose and extractives leads to an augmented cellulose content, thereby proportionately enhancing crystallinity [30]. The significant content of extractives in the camphor pruning under investigation markedly influences crystallinity.

### *3.4. Porosity Measurement*

Figure 5 illustrates the apparent density and porosity of BFIB produced under various applied pressures. At 2.0 MPa of applied pressure, the BFIB exhibits a maximum porosity of 15.47% and a minimum apparent density of 0.83 g/cm³. Conversely, when the applied pressure is 8.0 MPa, the BFIB demonstrates a minimum porosity of 5.08% and a maximum apparent density of 1.08 g/cm³. In comparison to alternative fiber insulation boards [31], BFIB exhibits a relatively low porosity at a similar density. This phenomenon arises because smaller porosity facilitates enhance hydrogen bonding among fiber molecules. The porosity of the BFIB gradually decreased as the applied pressure increased, while the apparent density slowly increased. However, when the applied pressure surpasses 6.5 MPa, the reductions in porosity and the gains in apparent density becomes less pronounced. This phenomenon occurs because heightened pressure expedites the removal of water molecules bound to the fibers through extrusion, and the application of heat further accelerates water

evaporation, resulting in the formation of stronger fiber bonds. Nevertheless, this effect does not imply that a sustained increase in applied pressure will consistently reduce the porosity or enhance the apparent density.

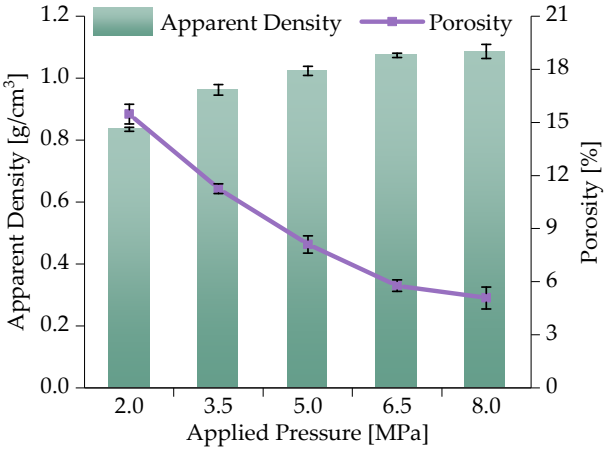


**Figure 5.** Apparent density and porosity of the BFIB under different applied pressure ($\rho < 0.05$).

Figure 6 depicts the density distribution variation of BFIB concerning the thickness interface. The density of each BFIB sample is axisymmetrically distributed in the board's center. To facilitate the analysis, the density profiles along their axes of symmetry are displayed. The BFIB samples produced in this work exhibit similar density distribution profiles. The thickness of the BFIB uniformly increased in apparent density in the range of 0 to 0.4 mm. Simultaneously, the increased rate in the apparent density of the BFIB was higher as the applied pressure became bigger. This is because the increase in the applied pressure reduces the volume of air and water molecules more quickly, allowing their internal structure to stabilize early. In the subsurface zone, which reached a thickness of about 0.4 mm, the apparent density distribution did not significantly fluctuate but was slowly stabilized and did not appear to have a slightly lower density in the core layer than in the surface layer. In this work, no chemical binders were added during the fabrication process of the BFIB, which relied only on the hydrogen and hydroxide bonds between the fibers to bond with each other. This approach avoids a density fluctuation phenomenon seen in adhesive build-up [32,33]. Concurrently, the BFIB was gradually formed from the core layer to the surface layer, with the moisture inside the insulation board being eliminated outwards through the surface layer or evaporated in the surface layer. This may result in the creation of larger voids and less apparent density in the surface layer of the BFIB relative to the core layer, a conclusion supported by SEM images.

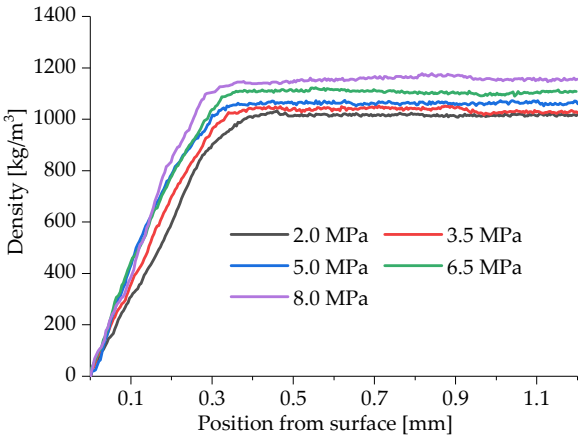


**Figure 6.** Density profiles of the BFIB pressed under different applied pressure.

### *3.5. Mechanical Properties*

Figures 7 and 8 illustrate the mechanical properties of various BFIB prepared under different applied pressures. In this work, the material's deformation characteristics were evaluated by measuring the bending and tensile modulus of elasticity (MOE) of the BFIB.

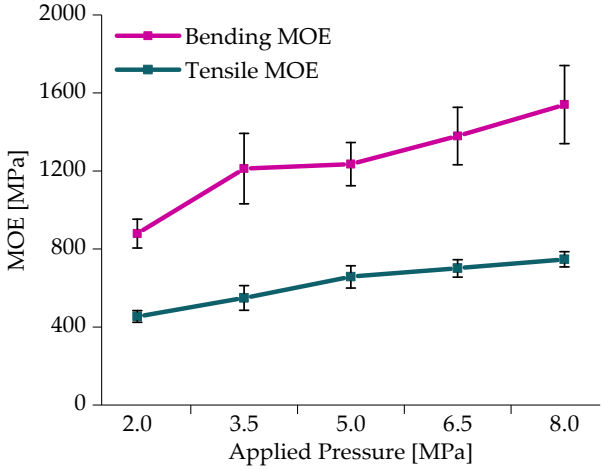


**Figure 7.** MOE of the BFIB produced under different applied pressure ($\rho < 0.05$).

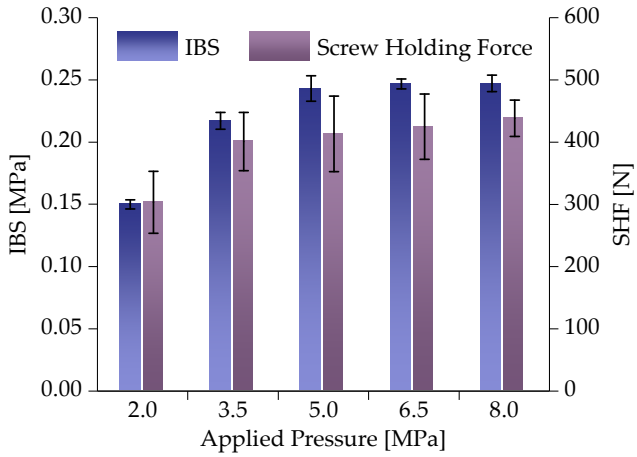


**Figure 8.** IBS and SHF of the BFIB produced under different applied pressure ($\rho < 0.05$).

From Figure 7, it is evident that the bending MOE nearly increases twice with the applied pressure, reaching a maximum of 1540.44 MPa at 8.0 MPa. However, the change in the tensile MOE is relatively small, with a maximum value of 747.84 MPa. The increased applied pressure brought camphor fiber molecules into closer contact, facilitating the formation of intermolecular hydrogen and hydroxide bonds among cellulose molecules. Simultaneously, this process mechanically entangled cellulose, potentially leading to the formation of intermolecular covalent bonds between cellulose molecules [34]. It is noteworthy that, compared to other binder-free fiberboards, the BFIBs in this work exhibited a relatively lower MOE. From compositional analysis-based studies, it has been revealed that pruned camphor branches contain a lower cellulose content, resulting in a reduced number of intermolecular hydrogen bonds and covalent bond formations between the fibers [35].

The IBS and SHF of BFIB produced under different applied pressures are presented in Figure 8. IBS, representing the breaking load per unit area of tensile strength perpendicular to the plane of the board, reflects the bond strength between the fibers. Notably, the IBS of the BFIB slowly increased as the applied pressure was raised from 2.0 to 5.0 MPa. However, when the applied pressure exceeded 5.0 MPa, the IBS was insignificantly changed, reaching a maximum of about 0.25 MPa. In comparison, the IBS values of conventional insulation

boards such as glass fiber and rock wool insulation boards generally fall in the range of 0.003 to 0.08 MPa [36]. Interestingly, Zhou et al. [3] used cotton stalk fibers to make an environmentally friendly insulation material, and Panyakaew et al. [1] employed coconut husk and bagasse to make a new type of thermal insulation board. Although in all these thermal insulation boards agroforestry wastes is used as a raw material, they possess lower bending MOE and IBS compared to BFIB.

Given the importance of SHF during BFIB installation in building applications, it is crucial to thoroughly assess its properties. Interestingly, the SHF does not continuously increase with the applied pressure; it does not significantly change when the applied pressure exceeds 5.0 MPa, reaching a maximum of 438.32 N. From the SEM images, it was observed that during the applied pressure range of 2.0~5.0 MPa, the BFIB surface camphor fiber arrangement gradually became regular and orderly, and the internal fibers became more compact. This result further validates the observed patterns in IBS and SHF. However, numerous tiny voids and gullies impede the bonding of hydrogen and hydroxide bonds between the fibers, affecting the overall performance of the BFIB. Beyond the applied pressure of 5.0 MPa, the changes in fiber arrangement became less conspicuous, and there was no significant difference between IBS and SHF at this stage. Compared to other materials, the SHF of bio-boards manufactured by using soybean straw by SONG et al. [25] was slightly lower than that of BFIB. This gives BFIB a comparative advantage in construction applications. Although BFIB is more advantageous in the same type of thermal insulation board compared with traditional thermal insulation materials, its mechanical properties are relatively weak, which is considered one of the main factors limiting its wide practical application.

### *3.6. Water Vapor Permeability*

As can be seen from Figure 9, both the WVTR and WVP of the BFIB decrease with the increase in the applied pressure. Particularly, when the applied pressure is 8 MPa, the WVTR is minimized to 224.79 g/($m^2$·24 h) and the WVP is minimized to 1.62 (g·cm)/($cm^2$·s·Pa). In this investigation, the primary moisture transfer mechanism within the BFIB is the diffusion of water vapour through air-filled pore spaces. This is in contrast to solid wood, where void distribution is relatively limited, and combined water diffusion is less prominent [37]. Importantly, it is worth noting that in this BFIB study, these tiny voids remain unaltered by chemical additives. The density distribution graph and SEM image provide concrete pieces of evidence for the existence of an intriguing phenomenon: while the void in the BFIB's surface layer was more substantial, offering ample room for water vapour molecules, the central layer's thickness consistently increased by raising the applied pressure.

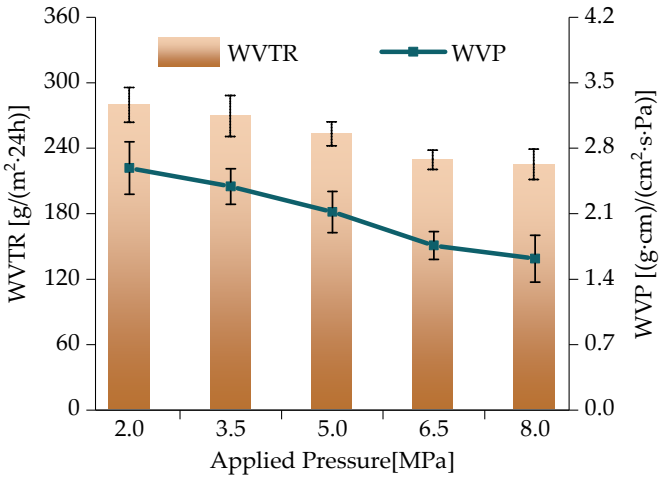


**Figure 9.** WVTR and WVP of the BFIB produced under different applied pressure ($\rho < 0.05$).

Furthermore, its density significantly exceeded that of the surface layer, suggesting a proportionately smaller void. This structural variation impedes the passage of water molecules, consequently leading to the continuous reduction in the water vapour permeability. WVP as an important indication of the moisture permeability of the BFIB is independent of the thickness of the material. The wood fibers themselves, as hydrophilic materials, facilitate the water vapour molecules to pass through. However, the increase in the applied pressure promotes the formation of hydrogen bonds between the fiber molecules; at the same time, the fibers are better aligned, which plays a role in dividing the voids inside the BFIB and acts as a hindrance to the water molecule transfer mechanism.

### *3.7. Thermal Conductivity Measurement*

Thermal conductivity serves as a crucial metric for evaluating the thermal efficiency of a material, enabling a quantitative comparison of various insulation materials [38]. Figure 10 illustrates the thermal conductivity of BFIB produced under varying conditions in this work. With rising the applied pressure, the thermal conductivity of BFIB exhibited a gradual increase, ranging from 0.086 to 0.096 W/(m·K). It remained consistent with the stipulated design criteria of JIS A5908: particleboards [39] for a thermal conductivity value lower than 0.15 W/(m·K). When compared to materials of a similar type, BFIB exhibited superior thermal insulation performance than wood (0.151 W/(m·K)) [40], although it fell short of inorganic materials such as rock wool (0.025–0.035 W/(m·K)) and glass fiber (0.034–0.047 W/(m·K)) [41]. Moreover, its thermal conductivity, within the same density range, aligned with that of a particleboard made from a blend of durian peel and coconut husk fiber (0.0728–0.1117 W/(m·K)) [6], demonstrating a similar determination result.

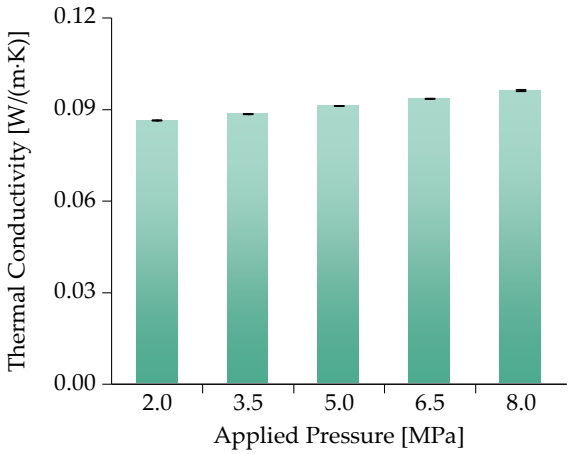


**Figure 10.** Thermal conductivity of the BFIB produced under different applied pressure ($\rho < 0.05$).

To consider the relationship between the porosity and thermal conductivity, a correlation analysis between the porosity and thermal conductivity of BFIB was performed as shown in Figure 11. It is evident from the graph that an increase in the porosity corresponds to a decrease in the thermal conductivity. This phenomenon can be attributed to the voids within the material, which act as scattering centers for phonons. Heat transfer occurs through both the solid material and these voids. Importantly, the thermal conductivity of the air within the voids is substantially lower than that of the solid material. This leads to an overall reduction in the material's thermal conductivity [42]. Consequently, a progressive rise in the applied pressure leads to higher density while diminishing its heat-insulating property.

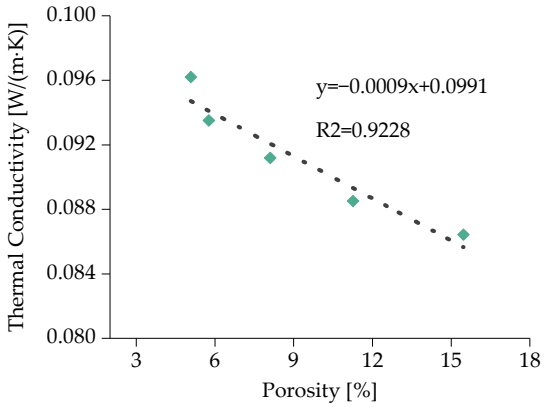


**Figure 11.** The correlation coefficient between thermal conductivity and porosity of BFIB.

### *3.8. Limiting Oxygen Index (LOI)*

Figure 12 presents the limited oxygen index (LOI) data for all BFIB samples. LOI serves as a commonly employed method for assessing the flame retardancy of thermal insulation materials. It is noteworthy that the limited oxygen index of BFIB exhibits a gradual increase under the application of higher applied pressure, consistently exceeding 22% for all values. As indicated in Table 3, these results affirm that BFIB, while combustible, possesses inherent self-extinguishing properties. It is essential to note that wood, as a material, is known for its flammability [43]. However, in this work, the physical enhancement of BFIB's flame retardancy without the addition of any chemical flame retardants was demonstrated. At 8 MPa of applied pressure, the LOI of BFIB reaches its peak at 26.14%, although it remains below 27%. This classification still placed it within the category of combustible yet self-extinguishing materials. Lau et al. [44] reported an LOI of 20.48% for particleboards comprising a blend of rice husk and wood particles, highlighting the enhanced flame retardancy of BFIB even in the absence of additional flame retardants.

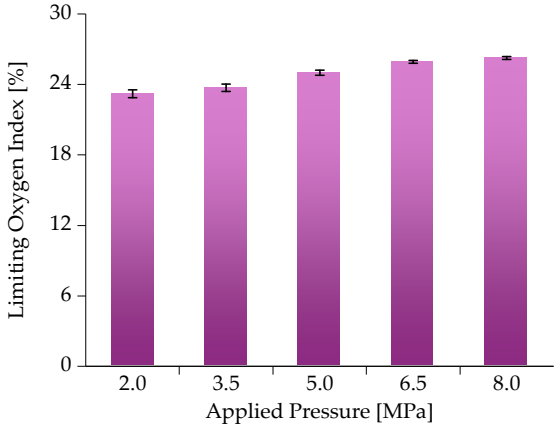


**Figure 12.** LOI of the BFIB produced under different applied pressure ($\rho < 0.05$).

**Table 3.** Properties of the LOI.

| LOI Level | Ignitability |
|---|---|
| ≤22 | Combustible |
| 23–27 | Self-extinguishing |
| ≥27 | Fire retardant |

Potential approaches for fire-retardant timber were reviewed, identifying two main approaches: char formation and isolating layers. Flame retardants, as the additive of choice for the isolating layers in wood fire retardation, are typically applied to the surface of the

wood or impregnated into the wood structure using vacuum pressurization techniques. While it is user-friendly and demands a relatively small amount of flame retardant for fire protection, this approach significantly extends the biodegradation period of wood following disposal [45]. The BFIB improves flame retardancy by char formation, which depends on a low-temperature dehydration reaction. BFIB removes most of the water during the production process, and, at the same time, the large number of voids in BFIB provides a large amount of oxygen for combustion. As a result, the pyrolysis of cellulose, hemicellulose, and lignin is accelerated, which produces a graphite carbon structure adhering to the BFIB to achieve the self-extinguishing effect of isolation from the air.

## 4. Conclusions

In this work, a novel thermal insulation material utilizing agroforestry waste as a raw material was introduced, aiming to replace traditional inorganic thermal insulation materials. Significantly, this material does not contain resins or other chemical additives, allowing for direct disposal into nature after use. This approach not only effectively addresses the challenge of agricultural and forestry waste disposal but also contributes to the recycling of carbon elements on the ground.

Porosity, which is regarded as a key factor influencing the performance of fiber insulation boards (BFIB), was thoroughly investigated by varying the applied pressure during production. A correlation between the density of BFIB under different conditions was established and the impact of porosity on thermal conductivity was discussed. As the applied pressure increased, porosity decreased from 15.47% to 5.08%, resulting in an inverse effect on the thermal conductivity, which increased from 0.086 to 0.096 W/(m·K). While a consistent increase in the applied pressure enhances the mechanical properties of BFIB to some extent, it comes at the expense of the increased thermal conductivity.

BFIB emerges as a promising insulator for energy-efficient building materials, and thermal and hygric behaviour properties position it as a viable competitor to other insulating materials, with the added advantage of causing no environmental harm post-use. The BFIBs in this work are suitable for use as thermal insulation in building walls or ceilings and do not play a load-bearing role in their application, which limits their application. Several drawbacks were also identified in this work, such as a lengthy production cycle, which seriously affects the economic efficiency of BFIB in the production process. In addition to this, the mechanical properties were lower compared to the insulation boards containing adhesives. Future research endeavors could explore potential methods to increase heating temperature and shorten the pressing times, where the melted lignin can act as a binder that works in conjunction with hydrogen and hydroxide bonding to make BFIB. Alternatively, the applied pressure during the pressing process could be reduced and biodegradable binders could be added to improve the insulation and mechanical characteristics of BFIB to replace inorganic insulation materials.

**Author Contributions:** Conceptualization, X.W. and C.C.; methodology, Z.C., X.S., T.G. and H.T.; software, Z.C.; validation, X.S., T.G. and H.T.; investigation, T.G.; resources, C.C.; data curation, Z.C. and X.S.; writing—original draft preparation, Z.C. and X.S.; writing—review and editing, X.W. and C.C.; supervision, X.W.; project administration, X.W. and X.S.; funding acquisition, X.W. and X.S. All authors have read and agreed to the published version of the manuscript.

**Funding:** This research was funded by JST, the establishment of university fellowships towards the creation of science technology innovation (JPMJFS2122), and the scientific research program of higher education in Inner Mongolia Autonomous Region (NJZZ23080).

**Data Availability Statement:** The data presented in this study are available on request from the corresponding author.

**Conflicts of Interest:** The authors declare no conflicts of interest.

## References


1. Panyakaew, S.; Fotios, S. New thermal insulation boards made from coconut husk and bagasse. *Energy Build.* **2011**, *43*, 1732–1739. [CrossRef]
2. Public Information and Research Project on Electricity Supply and Demand Measures in 2018. Available online: https://www.meti.go.jp/meti_lib/report/H30FY/000385.pdf (accessed on 18 October 2023).
3. Zhou, X.Y.; Zheng, F. An environment-friendly thermal insulation material from cotton stalk fibers. *Energy Build.* **2010**, *42*, 1070–1074. [CrossRef]
4. Wei, K.; Lv, C. Development and performance evaluation of a new thermal insulation material from rice straw using high frequency hot-pressing. *Energy Build.* **2015**, *87*, 116–122. [CrossRef]
5. Jelle, B.P. Traditional, state-of-the-art and ther future mal building insulation materials and solutions–Properties, requirements and possibilities. *Energy Build.* **2011**, *43*, 2549–2563. [CrossRef]
6. Khedari, J.; Nankongnab, N. New low-cost insulation particleboards from mixture of durian peel and coconut coir. *Build. Environ.* **2004**, *39*, 59–65. [CrossRef]
7. Khedari, J.; Charoenvai, S. New insulating particleboards from durian peel and coconut coir. *Build. Environ.* **2003**, *38*, 435–441. [CrossRef]
8. Binici, H.; Eken, M.; Kara, M. An environment-friendly thermal insulation material from sunflower stalk, textile waste and stubble fibers. In Proceedings of the International Conference on Renewable Energy Research and Applications (ICRERA), Madrid, Spain, 20 October 2013.
9. Paiva, A.; Pereira, S. A contribution to the thermal insulation performance characterization of corn cob particleboards. *Energy Build.* **2012**, *45*, 274–279. [CrossRef]
10. Thomson, A.; Walker, P. Durability characteristics of straw bales in building envelopes. *Constr. Build. Mater.* **2014**, *68*, 135–141. [CrossRef]
11. Shea, A.; Wall, K. Evaluation of the thermal performance of an innovative prefabricated natural plant fibre building system. *Build Serv. Eng. Res. Technol.* **2013**, *34*, 369–380. [CrossRef]
12. Lee, S.H.; Lum, W.C. Particleboard from agricultural biomass and recycled wood waste: A review. *J. Mater. Res. Technol-JMRT* **2022**, *20*, 4630–4658. [CrossRef]
13. Pędzik, M.; Janiszewska, D. Alternative lignocellulosic raw materials in particleboard production: A review. *Ind. Crop. Prod.* **2021**, *174*, 114162. [CrossRef]
14. Cetiner, I.; Shea, A.D. Wood waste as an alternative thermal insulation for buildings. *Energy Build.* **2018**, *168*, 374–384. [CrossRef]
15. Ferreira, G.; Thiex, N. Symposium review: Fiber and in vitro methods, analytical variation, and contributions to feed analysis. *J. Dairy Sci.* **2023**, *106*, 4464–4469. [CrossRef] [PubMed]
16. Miranda, M.T.; Arranz, J.I. Energetic characterization of densified residues from Pyrenean oak forest. *Fuel* **2009**, *88*, 2106–2112. [CrossRef]
17. El Oudiani, A.; Chaabouni, Y. Crystal transition from cellulose I to cellulose II in NaOH treated *Agave americana* L. fibre. *Carbohydr. Polym.* **2011**, *86*, 1221–1229. [CrossRef]
18. Segal, L.G.J.M.A.; Creely, J.J. An empirical method for estimating the degree of crystallinity of native cellulose using the X-ray diffractometer. *Text. Res. J.* **1959**, *29*, 786–794. [CrossRef]
19. *JIS A. 5905*; Japanese Industrial Standards. Fiberboards: Tokyo, Japan, 2014.
20. McCurdy, C.; Dixion, D. A Comparison of the Sealing, Forming and Moisture Vapour Transmission Properties of Polylactic Acid (PLA), Polyethene (PE) and Polyethylene Terephthalate (PET) Coated Boards for Packaging Applications. *J. Packag. Technol. Res.* **2022**, *6*, 91–100. [CrossRef]
21. *JIS Z. 0208*; Japanese Industrial Standards, Testing Methods for Determination of the Water Vapour Transmission Rate of Moisture−Proof Packaging Materials (Dish Method). Fiberboards: Tokyo, Japan, 1976.
22. *ISO 22007-6*; Comparative Method for Low Thermal Conductivities Using a Temperature-Modulation Technique. International Organization for Standardization: Geneva, Switzerland, 2014.
23. *JIS K 7201-2*; Japanese Industrial Standards, Plastics−Determination of Burning Behaviour by Oxygen Index−Part 2: Ambient-Temperature Test. Fiberboards: Tokyo, Japan, 2007.
24. Field, A.P. Discovering Statistics Using SPSS: (and Sex, Drugs and Rock'N'Roll). No Title 2005, xxxiv. Available online: https://cir.nii.ac.jp/crid/1370848662539321089 (accessed on 18 October 2023).
25. Song, X.; Wang, X. Effects of heating temperature on the properties of bio-board manufactured by using soybean straw. *Materials* **2020**, *13*, 662. [CrossRef]
26. Nasir, M.; Khali, D.P. Recent development in binderless fiber-board fabrication from agricultural residues: A review. *Constr. Build. Mater.* **2019**, *211*, 502–516. [CrossRef]
27. Shi, J.; Zhong, T. Eco-friendly and special-shaped bamboo binderless fiberboards fabricated by self-bonding technology: Effect of bamboo fibers with different sizes. *Ind. Crop. Prod.* **2023**, *194*, 116300. [CrossRef]
28. Yin, J.; Yuan, T. Effect of compression combined with steam treatment on the porosity, chemical compositon and cellulose crystalline structure of wood cell walls. *Carbohydr. Polym.* **2017**, *155*, 163–172. [CrossRef] [PubMed]
29. Hu, J.P.; Guo, M.H. Influence of ammonium lignosulfonate on the mechanical and dimensional properties of wood fiber biocomposites reinforced with polylactic acid. *Ind. Crop. Prod.* **2015**, *78*, 48–57. [CrossRef]

30. Ji, X.; Dong, Y. Environment-friendly wood fibre composite with high bonding strength and water resistance. *R. Soc. Open Sci.* **2018**, *5*, 172002. [CrossRef] [PubMed]
31. Rebolledo, P.; Cloutier, A. Effect of density and fiber size on porosity and thermal conductivity of fiberboard mats. *Fibers* **2018**, *6*, 81. [CrossRef]
32. Gumowska, A.; Kowaluk, G. Physical and Mechanical Properties of High-Density Fiberboard Bonded with Bio-Based Adhesives. *Forests* **2023**, *14*, 84. [CrossRef]
33. Boruszewski, P.; Borysiuk, P. The influence of laccase modifications of lignin on the properties of biocomposites from natural-fiber material with lignins as binder. In Proceedings of the International Conference on Environmental Engineering and Applications (ICEEA 2011), San Francisco, CA, USA, 21 October 2011.
34. Quintana, G.; Velasquez, J. Binderless fiberboard from steam exploded banana bunch. *Ind. Crop. Prod.* **2009**, *29*, 60–66. [CrossRef]
35. Ramos, D.; El Mansouri, N.E. All-lignocellulosic fiberboard from steam exploded *Arundo donax* L. *Molecules* **2018**, *23*, 2088. [CrossRef]
36. Pfundstein, M.; Gellert, R. Statutory instruments and insulating material standards. In *Insulating Materials: Principles, Materials, Applications*, 1st ed.; Christina, S., Ed.; Birkhäuser: Munich, Germany, 2008; pp. 59–74.
37. Sonderegger, W.; Niemz, P. Thermal conductivity and water vapour transmission properties of wood-based materials. *Eur. J. Wood Wood Prod.* **2009**, *67*, 313–321. [CrossRef]
38. Al-Homoud, M.S. Performance characteristics and practical applications of common building thermal insulation materials. *Build. Environ.* **2005**, *40*, 353–366. [CrossRef]
39. *JIS A. 5908*; Japanese Industrial Standards. Particleboards: Tokyo, Japan, 2015.
40. Xu, J.; Sugawara, R. Manufacture and properties of low-density binderless particleboard from kenaf core. *J. Wood Sci.* **2004**, *50*, 62–67. [CrossRef]
41. Zou, N.Y. *Thermal Insulation Materials for Wall and Roof*; Chemical Industry Publish House: Beijing, China, 2008.
42. Suleiman, B.M.; Larfeldt, J. Thermal conductivity and diffusivity of wood. *Wood Sci. Technol.* **1999**, *33*, 465–473. [CrossRef]
43. Li, B.; He, J. Investigation of mechanical property, flame retardancy and thermal degradation of LLDPE–wood-fibre composites. *Polym. Degrad. Stabil.* **2004**, *83*, 241–246. [CrossRef]
44. Lau, H.L.; Lamaming, J. Synergistic influence of flame retardant additives and citric acid on the functional properties of rice husk/wood blended particleboards. *Maderas-Cienc. Tecnol.* **2021**, *37*, 1–10. [CrossRef]
45. Lowden, L.A.; Hull, T.R. Flammability behaviour of wood and a review of the methods for its reduction. *Fire Sci. Rev.* **2013**, *2*, 4. [CrossRef]


**Disclaimer/Publisher's Note:** The statements, opinions and data contained in all publications are solely those of the individual author(s) and contributor(s) and not of MDPI and/or the editor(s). MDPI and/or the editor(s) disclaim responsibility for any injury to people or property resulting from any ideas, methods, instructions or products referred to in the content.